HIGH ANGLE OF ATTACK APPROACH AND LANDING CONTROL LAW DESIGN FOR THE X-31A

B. Fischer and Dr. A. Knoll
European Aeronautic Defense and Space Company
Military Aircraft
Flight Dynamics
81663 Munich, Germany

Keywords: *ESTOL, X-31A, CONTROL LAWS, VECTOR*

Abstract

The X-31 flight control system enables flying at very high angles of attack, including the poststall regime. This not only offers extreme maneuverability, but also the capability for a steady slow flight. This feature can also be used for the landing approach. Since the landing ground roll distance is proportional to the square of the speed during touchdown, reducing the speed offers a crucial advantage with regard to landing performance. The X-31 VECTOR program is developing and flight-testing this new technique with the automatic Extreme Short Takeoff and Landing (ESTOL).

The following presentation shows the development of the ESTOL autopilot control laws, based on the standard X-31 control laws, starting from the design objectives, leading to the present structure. The calculation of the flight path as well as the feedback and the feedforward path for both the longitudinal and the lateral axis are described.

The control laws during the derotation phase, immediately before touch down are also presented.

Time histories demonstrate the quality of the present solution.

1 Introduction

1.1 The VECTOR Program

The Vectoring, ESTOL Control and Tailless Operation Research (VECTOR) project has been launched by the U.S. Navy and the German Federal Office for Defense Technology and Procurement (BWB) with Boeing and EADS Military Aircraft as industry prime contractors.

The concept of ESTOL offers the potential to dramatically reduce the landing speeds and energy levels for fighter aircraft. Especially for carrier operations, wind over deck requirements for landing could be reduced.

Reduction of landing distances can be achieved by flying an approach at an increased angle of attack (AoA) up to and potentially beyond the stall angle of attack. This is followed by a derotation phase close to the ground in order to reduce the aircraft's pitch attitude to a value that ensures sufficient tail clearance at touch down. This derotation phase also has to assure, that vertical speed at touch down does not exceed its maximum allowed value. Due to these challenging demands the maneuver is conducted fully automatically.

To investigate the short landing capabilities, the aircraft has been upgraded with:

- An Integrity Beacon Landing System (IBLS©) from Palo Alto, California based company IntegriNautics.
- An autothrottle system
- A flight control software for high AoA approaches and landings.

These control laws, also called ESTOL control laws or ESTOL autopilot, are designed using a feed forward/feedback philosophy and are integrated into the existing X-31A control laws.

2 Objectives and Basic Requirements

2.1 X-31A Aircraft Configuration

The X-31A is a single seat longitudinal unstable aircraft with a delta-canard configuration. It has a GE F404-400 engine with afterburner, producing 16000 lbs. of thrust at sea level.

Figure 1 depicts the control effectors of the X-31A including aerodynamic and thrust-vectoring control deflectors.

The primary aerodynamic control surfaces are the symmetric trailing edge flaps and the canards for the longitudinal axis and the differential trailing edge flaps and rudder for the lateral/directional axes. Additionally, a thrust vectoring system is used to augment the aerodynamic control power during low speed and poststall flight. The deflections of the leading edge slats are scheduled with the angle of attack and are fully extended for poststall flight.

2.2 Design task

An ESTOL maneuver consist of three segments (Figure 2):

1. Descent at high angle of attack (AoA)
2. Derotation after reaching minimum tail height
3. Touch down and roll out

To ensure proper operation of the ESTOL autopilot it is important to know the position of the aircraft accurately. Therefore, the aircraft position is determined by blending IBLS© position data with data from the Inertial Navigation System (INS), which provides up to cm-level accuracy. To achieve this high accuracy, a pass through an imaginary bubble, defined by two ground based integrity beacon transmitters (pseudolites) is necessary.

Therefore, a complete ESTOL approach pattern consists of two parts: First, a manual flight through the IBLS© bubble followed by a manually flown traffic pattern into the "ESTOL engagement box". Second, if all the ESTOL related criteria are met, the pilot can engage the autopilot (Figure 2). Then the autopilot will guide the airplane along the commanded trajectory during the approach and the landing phase including touchdown.

2.3 Design Objectives

The ESTOL autopilot has to meet the following design objectives:

- Closed loop stability
- Satisfactory tracking performances
- Robustness against turbulence and gusts
- Flexible trajectory command
- Flexible AOA build-up
- Sufficient tail ground clearance
- Vertical speed at touch down below maximum permitted vertical speed
- Wave-off capability.

3 General Control Law structure

Figure 3 shows the general control law structure of the X-31. On the left side all sensor inputs are shown providing the following signals for the control calculations:

- Rates and accelerations
- Position and the direction cosines
- Aerodynamic flow angles
- Airspeed, Mach number, dynamic pressure and altitude

The signals from the aerodynamic and the inertial sensors are mixed to get the flow angles and the velocity used in the control laws (see also [1]).

The measured position and the direction cosines provided by the INS and IBLS© are transformed into a fixed runway coordinate system. These additional signals are only used by the ESTOL autopilot.

3.1 Lateral/directional Autopilot

As shown in Figure 3, the lateral/directional autopilot is added as an outer loop to the basic lateral controller. The autopilot controls the lateral deviation Dy, the track angle c and the roll angle m and compensates for crosswind (Figure 4). The deviations of these parameters from the commanded values are used as commands for the basic control laws instead of the stick and pedal inputs (Figure 5).

3.2 Longitudinal Autopilot

The trajectory and the longitudinal control parameters of the ESTOL approach are shown in Figure 6. Both, stabilization of the aircraft and trajectory tracking are realized in an integrated inner loop design.

The existing longitudinal control laws have been extended by additional control signals, as

shown in Figure 9. The added ESTOL control laws consist of a feedforward path (called "Longitudinal ESTOL feedf orward control" in Figure 9) and a feedback path.

Due to the demanding design specifications for the longitudinal axis, the ESTOL autopilot features direct link commands to the control effectors.

3.2.1 Feedforward path

In the feedforward path (Figure 7) the command signals for AoA, pitch rate, altitude, speed, flight path and the curvature of the trajectory are calculated. This calculation consists of two independent parts: The trajectory determination yie lds the commanded altitude and the commanded flight path angle, while the AoA command calculation provides the commanded angle of attack. Using these signals, the commanded velocity and pitch rate can be derived. Furthermore, the direct link control signals to the trailing edge flaps, the canards and the autothrottle are calculated as a steady state inversion of the commanded AoA, airspeed, altitude and pitch rate.

3.2.2 Trajectory calculation

The trajectory is calculated in a fixed runway coordinate system. It consists of the following elements:

- Level flight within predefined altitude limits
- Descent with a constant flight path angle
- Level flight at derotation altitude

The specifications for the trajectory are:

- A smooth change between the trajectory elements
- No steps in accelerations
- Terrain clearance must be independent from wind conditions due to fixed reference to ground distance
- Flexibility to change the commanded flight path during flight tests

To meet these specifications, the trajectory consists of the following geometric elements:

- Straight line, for constant flight path
- Circle, for change in flight path angle (constant $\dot{g}$)
- 3rd order parabola, which gives a continuous transition from a straight line to a circle due to continuous cha nge in curvature

The trajectory is calculated in real time according to the actual altitude at engagement. This results in a wide altitude range for the ESTOL engagement.

The resulting signals are altitude command h_C and flight path angle command g_C which are used for the feedback control.

3.2.3 AoA command calculation

Independent from trajectory calculation, the AoA command is calculated. The AoA build up is defined by four AoA -rate break points along the trajectory and the desired final AoA. An early or late AoA build up can be commanded by shifting the break points. In Figure 8, the AoA rate and the resulting AoA - command versus distance to the derotation point is shown.

By using the results of the trajectory calculation and the AoA command calculation, the following command and direct link signals are calculated:

- Angle of attack command a_C
- Pitch rate command q_C
- Altitude command h_C
- Airspeed command V_C
- Flight path angle command g_C
- Trailing edge direct link signal d_{TEDL}
- Canard direct link signal, d_{CANDL}
- Power lever direct link signal, PLA_{DL}

3.3 Feedback path

The structure of the longitudinal feedback design is shown in Figure 9. For a better visibility, it was decided to split the stabilization part from the trajectory tracking part.

The basic longitudinal control law structure, featuring AoA (proportional and integral) and pitch rate feedback, is supplemented by additional feedback paths of airspeed, altitude (proportional and integral) and flight path angle. Additionally the ESTOL

controller provides an output to the autothrottle. Because of model uncertainties it is not possible to achieve zero steady state error in AoA, airspeed, flight-path angle and altitude simultaneously. Hence, a washout filter is included in the airspeed feedback path to filter out steady state errors.

The control power used for stabilization is collected in bottleneck 1 (point 1 in Figure 9). From there, the control power is distributed to the three longitudinal control surface signals.

The control power used for trajectory tracking (minus the autothrottle portion) is collected in bottleneck 2 (point 2 in Figure 9) and is distributed to the control surface signals.

To avoid steady state errors in the feedback signals, integrals of the AOA and altitude are included. To improve gust rejection and to relieve the integrators disturbance feedforward commands are added to the control effectors. For this the additional AoA due to wind (a_W) is calculated by subtracting the noseboom AoA a_{NS} from the AoA calculated from the inertial speeds a_{IN}.

3.4 Derotation phase

The derotation phase is triggered by undershoot of the minimum tail clearance h_{Tmin}. The purpose of this phase is to keep the tail above h_{Tmin}. (Figure 10). To achieve this, the aircraft has to rotate around the lowest point of the tail until touch down. Additionally the sink rate at touch down must not exceed the load limits of the landing gear.

During derotation the same feedback structure and gains as in the approach phase are used to avoid switching transients in the control laws. The five command signals, used for trajectory tracking are initialized to their last value before derotation.

During derotation, the command signals are calculated as shown in Figure 11:

Since the most demanding constraint during derotation is the tail clearance, all the command signals (except the airspeed command which stays constant) are derived from a new command signal: the pitch attitude command q_C.

$$q_C = q_0 + C_1 \cdot \int \dot{q}_C \, dt + C_2 \cdot \Delta h_T \qquad (1)$$

q_0 is the current pitch attitude. It is calculated from the altitude of the center of gravity h_{cg} and the tail height h_T (Figure 12):

$$q_0 = \arcsin\left(\frac{h_{cg} - h_T}{r_T}\right) - q_T \qquad (2)$$

The angle q_T between the lever arm r_T and the aircraft symmetry axis is subtracted for transformation into the aircraft body axis system.

$\dot{q}_C$ is the commanded pitch rate around the tail. It is calculated so that the velocity vector is divided into a transformation along the X-axis and a rotation around the tail (Figure 12):

$$\dot{q}_C = \frac{V_K \, g}{r_T \cdot \cos(q_0 + q_T)} \qquad (3)$$

For the 3rd part the tail undershoot Δh_T is calculated. It is negative if the tail is below h_{Tmin} while remaining zero if the tail is above h_{Tmin}. This provides an additional pitch down moment if the tail height falls below h_{Tmin}.

4. Moding

Once the ESTOL autopilot is engaged there are three modes as shown in Figure 13:

1. ESTOL AP mode
   This is the main mode if there are no failures. The aircraft tracks the trajectory and lands automatically.
2. Wave-off with autothrottle engaged
   If it is required to abort the ESTOL approach, an automatic wave off maneuver can be initiated.
   This mode can be engaged manually (by pushing the WAVE OFF button or by exceeding the throttle breakout force) or automatically (by exceeding ESTOL limits or failure detection).
   The throttle is set to MIL power if the wave off was not initiated by an autothrottle failure.
3. Wave off with manual throttle

If there was an autothrottle failure the autopilot switches to the wave off mode but the pilot has to manually control the power lever. All wave offs result in a wings level climbing flight with constant AoA. The pilot can disengage the autopilot at his discretion.

5. Analysis

To evaluate the ESTOL controller performance a 6-DOF nonlinear simulation was set up. Figure 14 shows the time histories for an approach with the ESTOL autopilot engaged from nonlinear simulation. Sensed and commanded altitude show an almost zero control error during the entire ESTOL maneuver. A similar good result is achieved for the AoA curves. Regarding the speed time histories, the effect of the washout filter in the feedback path can be seen. The actual speed V_S shows a nearly constant offset to the command signal V_C.

6. Acknowledgement

The subject of this paper is part of the VECTOR program conducted at the Naval A ir Station in Patuxent River, Maryland, USA by the US Navy, BWB, EADS Military Aircraft, Boeing and DLR.

References

[1] Beh, H.; Hofinger, G.: *Control Law Design of the Experimental Aircraft X-31A*, ICAS-94-7.2.1, ICAS Proceedings 1994, Anaheim, California, U SA

[2] Selmon, J. et al: *High Angle of Attack Autonomous Landing Using the X-31A Aircraft*, AIAA GNC Conference 2001

Figures

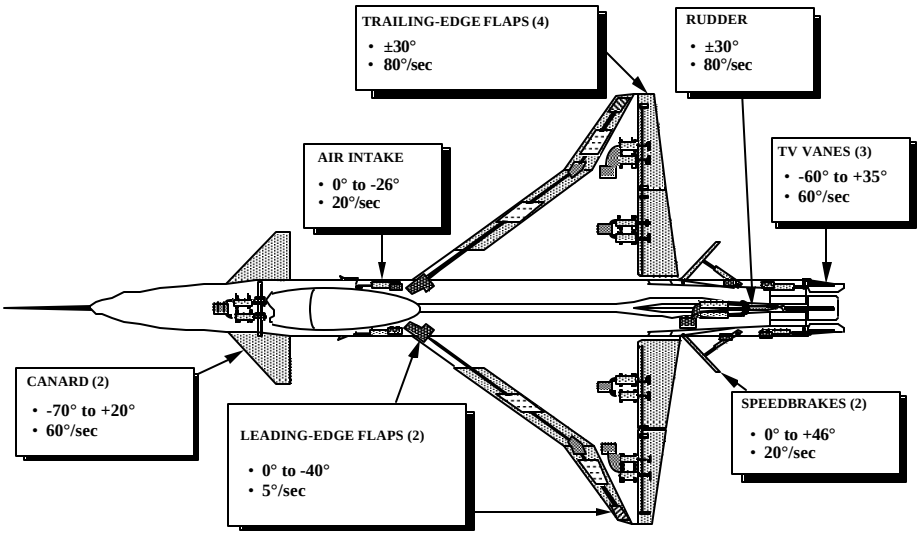

Figure 1: X-31A control surfaces

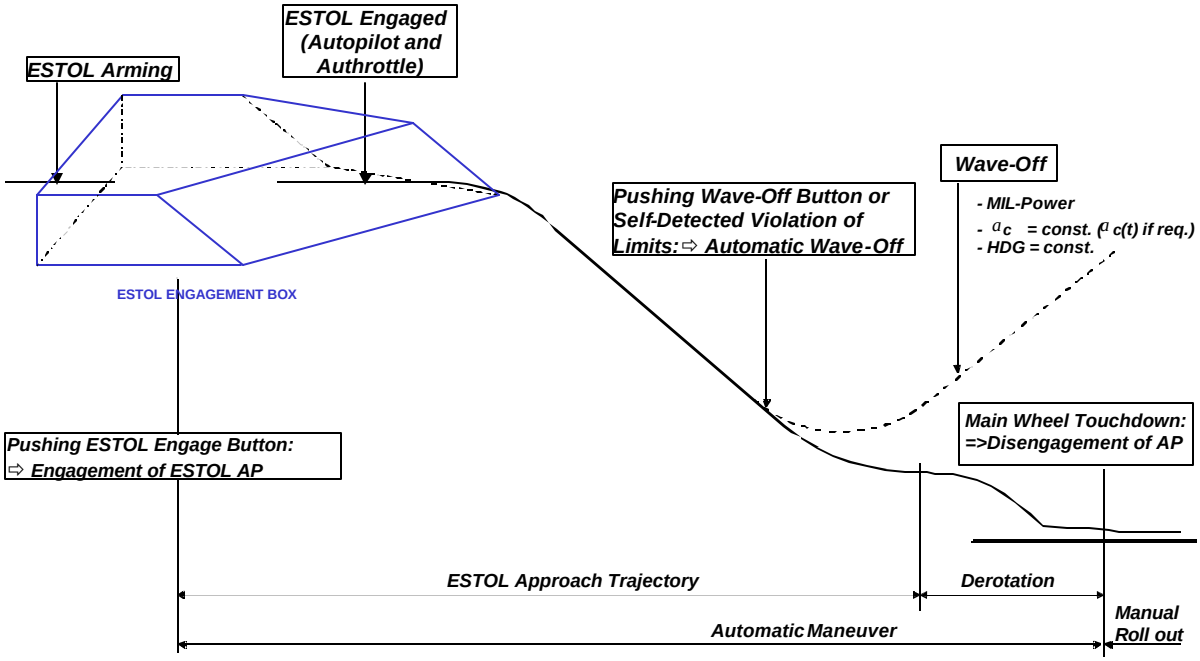

Figure 2: ESTOL approach and landing scheme

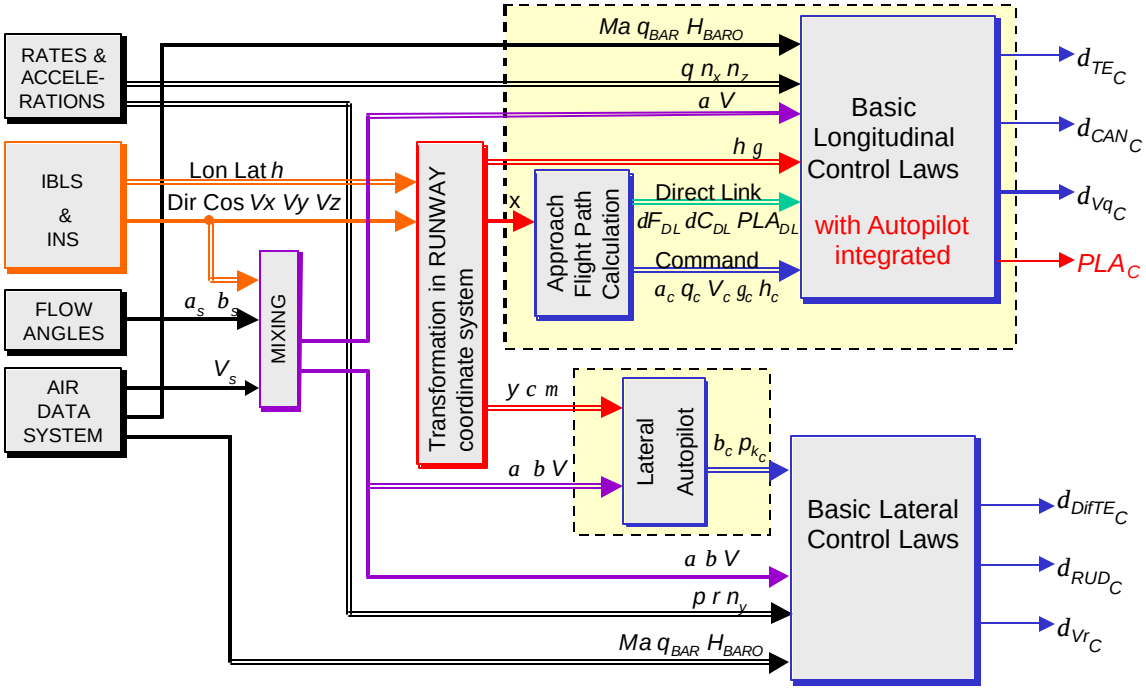

Figure 3: General control law structure

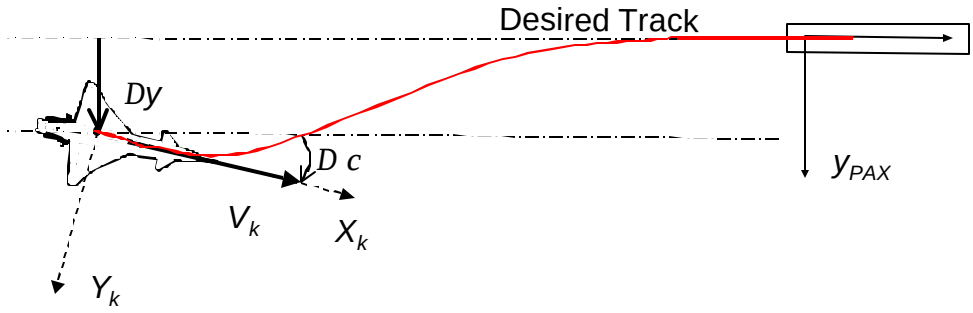

Figure 4: Lateral/directional control parameters

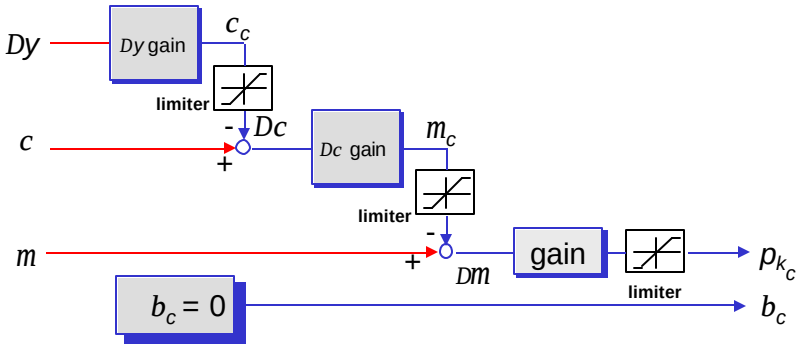

Figure 5: Lateral/directional autopilot control structure

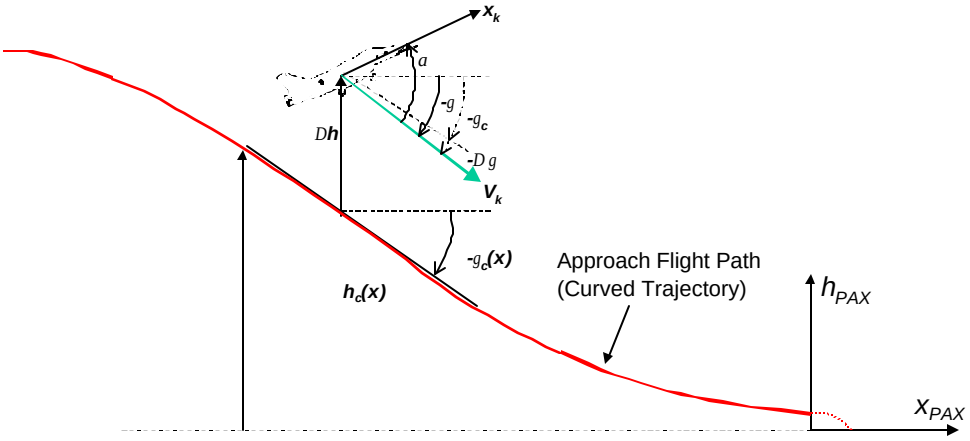

Figure 6: Longitudinal control parameters

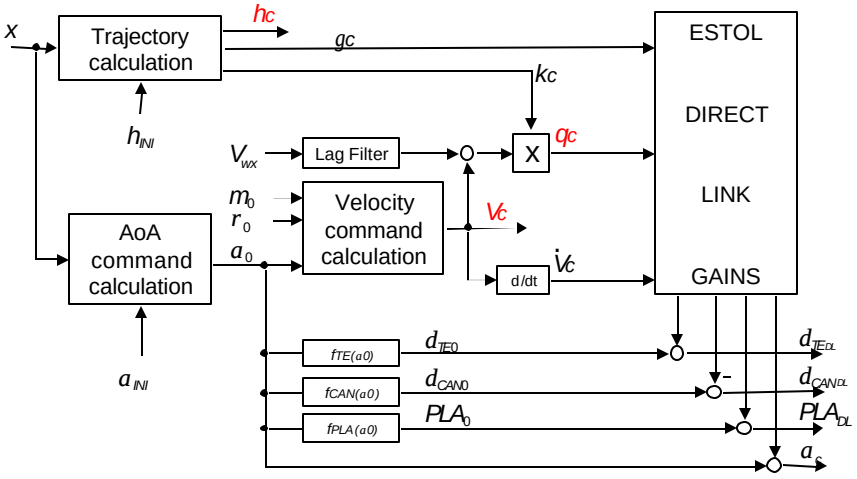

Figure 7: Longitudinal autopilot feedforward control structure

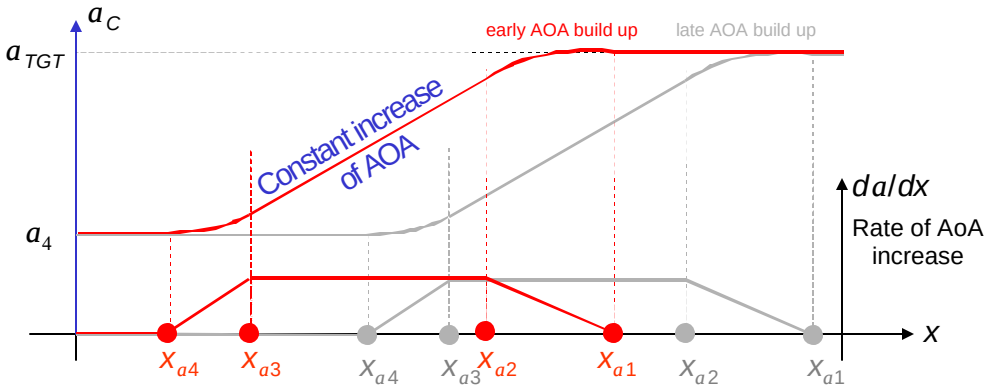

Figure 8: AoA build up calculation

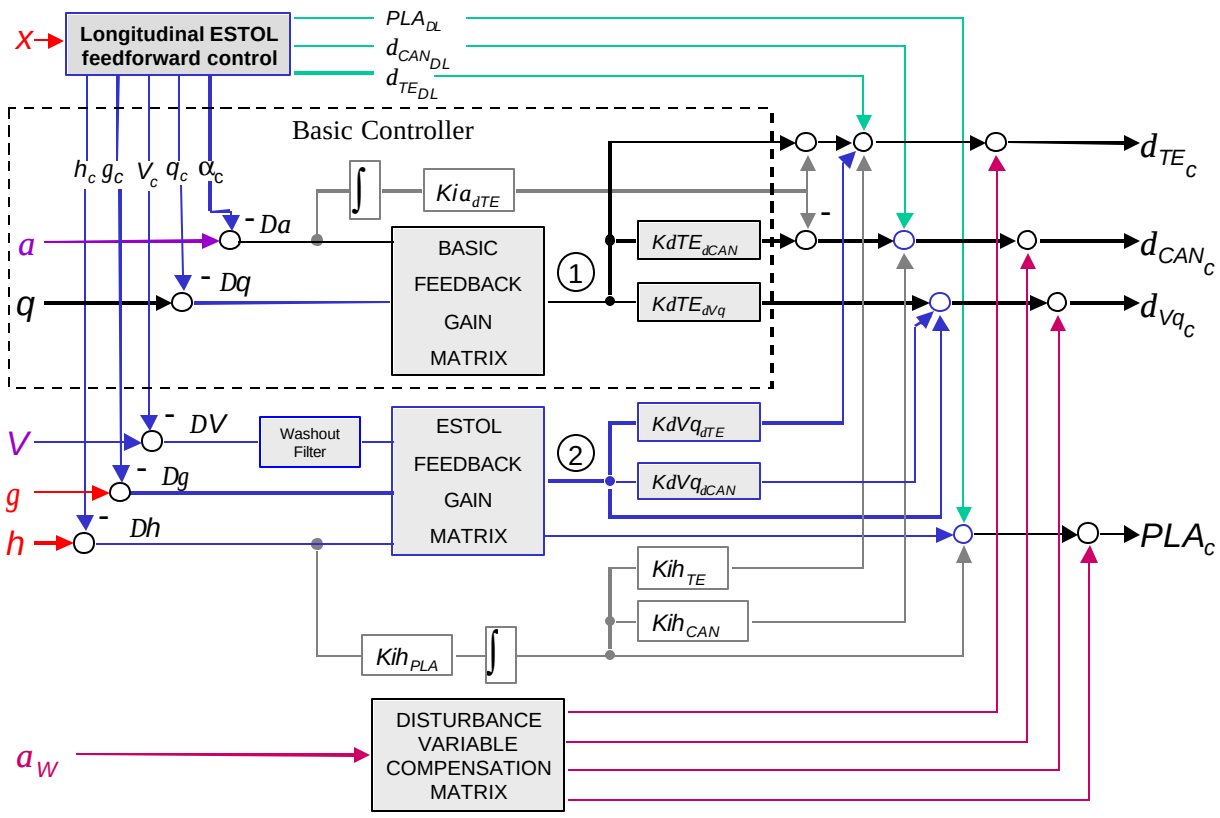

Figure 9: Longitudinal autopilot control law structure

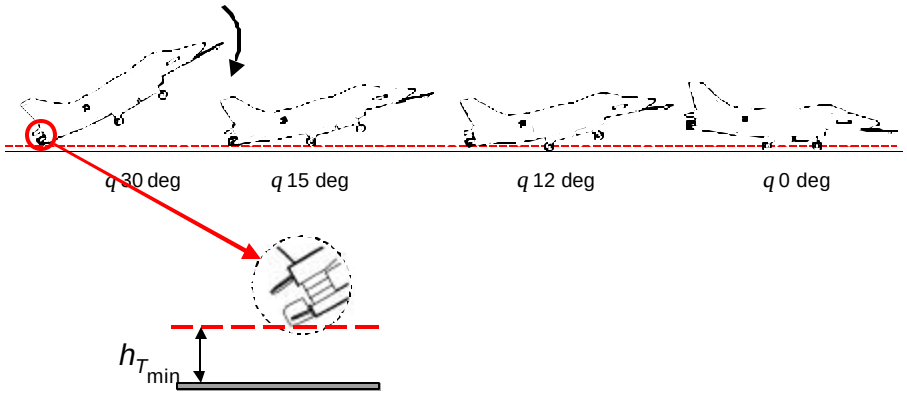

Figure 10: Tail height in derotation phase

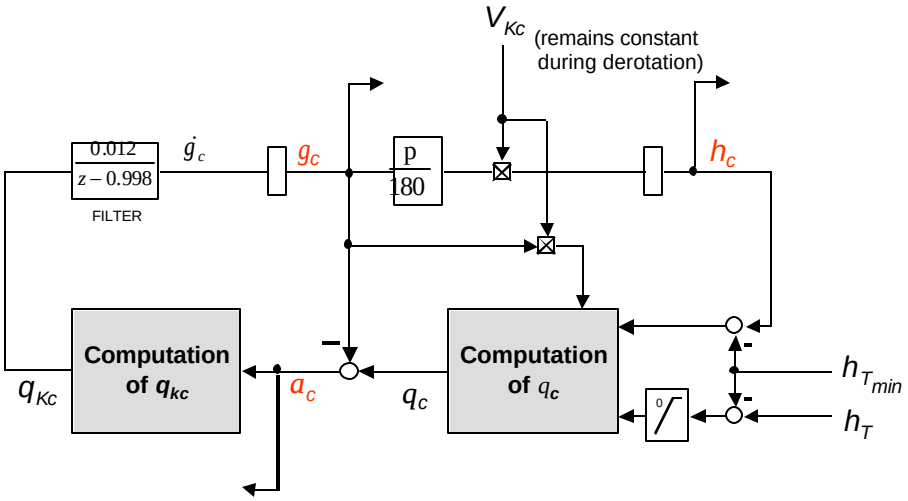

Figure 11: Calculation of command signals in derotation phase

$$q_0 = \text{asin}((h_c - h_T)/r_T) - q_T$$

$$\dot{q}_c = (V_{kc}\, g_c)/(r_T \cos(q_0 + q_T))$$

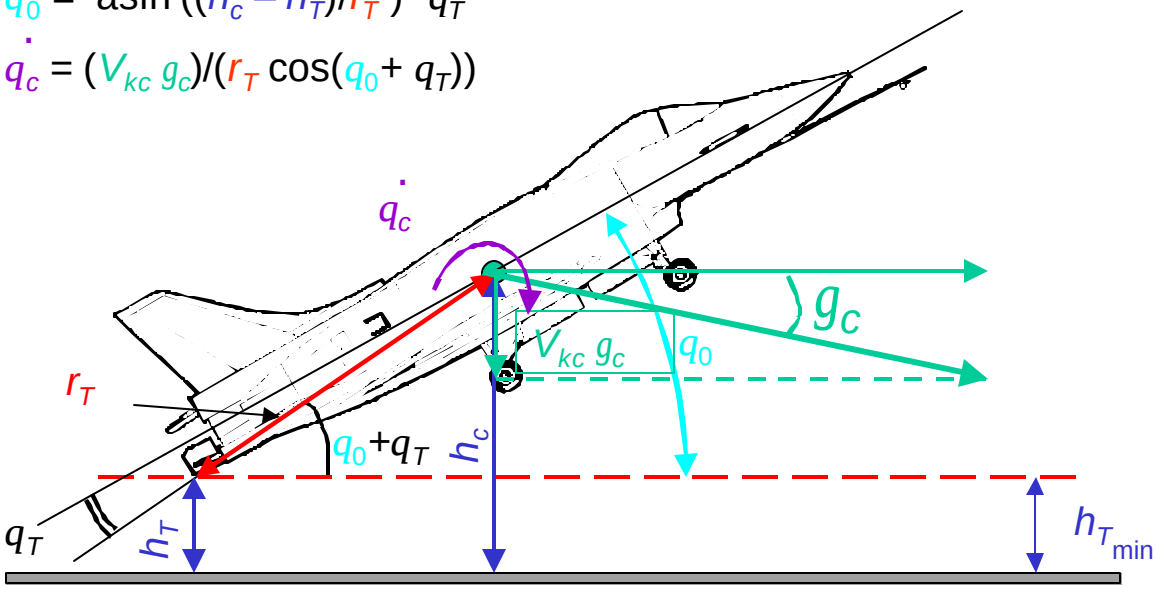

Figure 12: Angles and rates in derotation phase

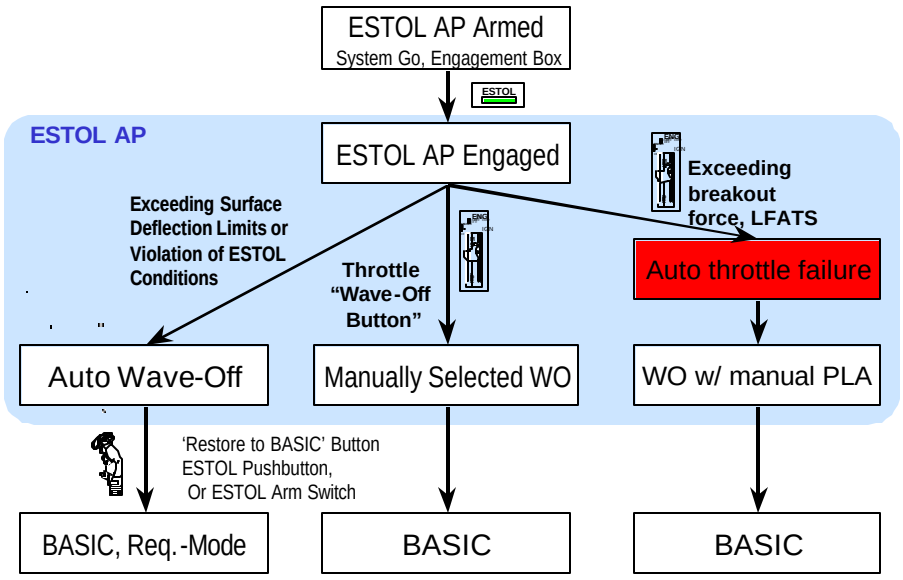

Figure 13: Modes of the ESTOL autopilot

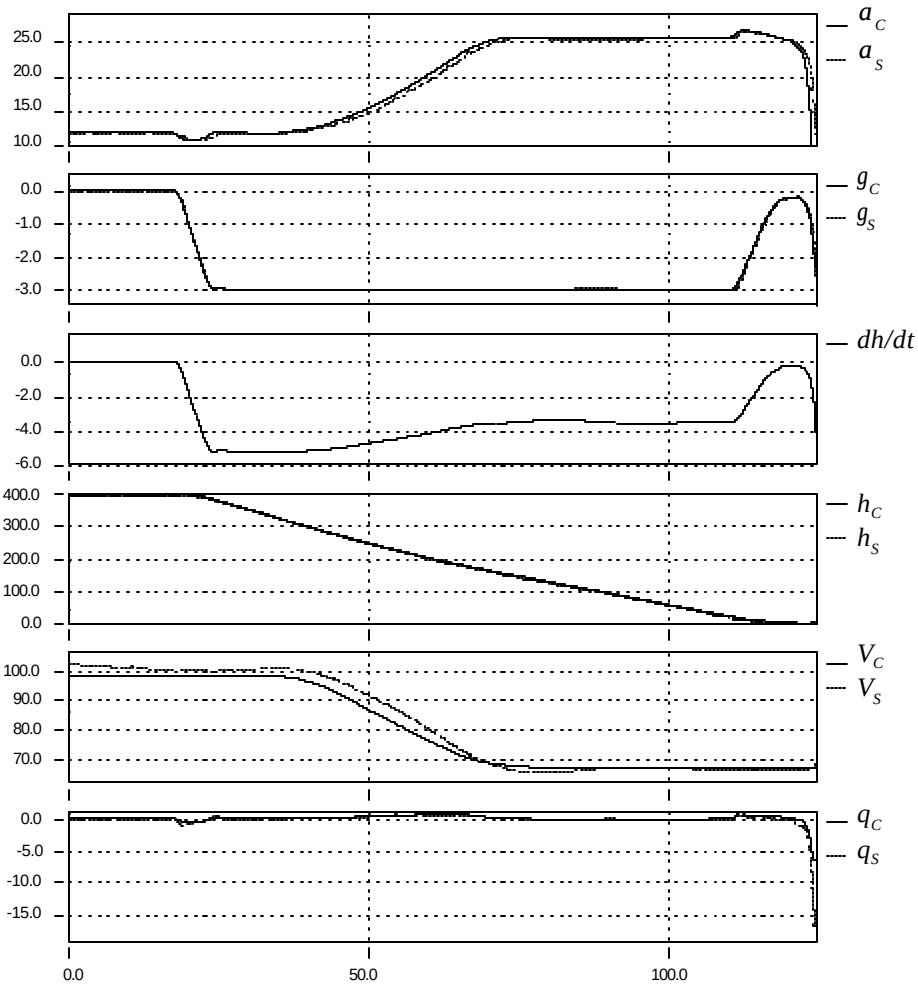

Figure 14: Nonlinear simulation of an ESTOL approach